MEASUREMENTS OF BEAM PULSE INDUCED MECHANICAL STRAIN INSIDE THE SNS* TARGET MODULE

W. Blokland†, M. Dayton, Y. Liu, B. Riemer, M. Wendel, D. Winder, Oak Ridge National Laboratory, Oak Ridge, USA

Abstract

Because several of the SNS targets have had a shorter lifetime than desired, a new target has been instrumented with strain sensors to further our understanding of the proton beam's mechanical impact. The high radiation and electrically noisy environment led us to pick multi-mode fiber optical strain sensors over other types of strain sensors. Special care was taken to minimize the impact of the sensors on the target's lifetime. We also placed accelerometers outside the target to try correlating the outside measurements with the internal measurements. Remote manipulators performed the final part of the installation, as even residual radiation is too high for humans to come close to the target's final location. The initial set of optical sensors on the first instrumented target lasted just long enough to give us measurements from different proton beam intensities. A second set of more rad-hard sensors, installed in the following target, lasted much longer, to give us considerably more data. We are developing our own rad-hard, single-mode fiber optic sensors. This paper describes the design, installation, data-acquisition system, the results of the strain sensors, and future plans.

INTRODUCTION

The Spallation Neutron Source uses neutron scattering to study the structure and properties of materials and macromolecular and biological systems. Proton beam pulses of less than 1 μs long, up to 24 μC, hit a stainless steel vessel filled with mercury at 60 Hz for a total power of up to 1.4 MW to generate the neutrons. The beam creates an initial pressure field of up to ~34 MPa that leads to tension and cavitation of the mercury as the pressure wave interacts with the target vessel.

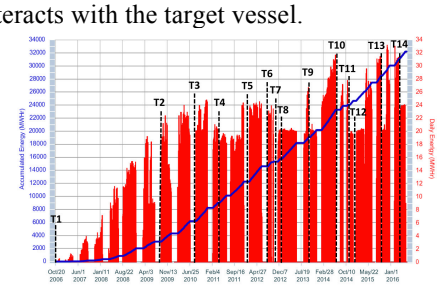

Figure 1: The SNS production runs.

The reliability of the target vessel is critical for minimizing interruptions to the operation schedule. It was initially thought that the lifetime of a target would be limited by the erosion of the target wall, due to the cavitation of the mercury during the proton beam impact, and by reaching the SNS administrative radiation damage limit of the vessel's steel at about 5000 MWHrs.

However, at higher proton beam powers, we did start seeing target failures before the radiation damage limit. Four out of seven premature target failures were due to weld failures from fatigue, while two were due to cavitation erosion, and one could not be determined. Figure 1 shows the quick succession of installation of targets 10, 11, and 12.

We decided to measure the strain on the actual target vessel wall to better understand the limitations to the target lifetime: Do the pulses induce a higher strain on the target than expected and does the repetition rate of the beam hit a resonance? Once we have a strain measurement system in place, we can see if certain mitigation methods are effective. In particular, we are interested in how effective injecting gas bubbles is at reducing the pressure wave. Also, we know that during operation an internal baffle erodes and a partial, non-critical, crack occurs. We hope that with a long-lasting strain sensor, we can find the point in time when this crack occurs.

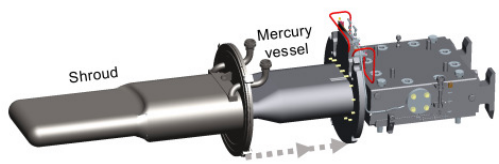

Figure 2: The target layout showing the shroud sliding over the mercury vessel.

The pulse-induced strain on liquid metal targets has been measured previously for the SNS target at LANL [1] and for displacement measurements of the J-PARC target [2], but not for the actual SNS target during beam impact. The SNS target has a double containment design, see Figure 2, and the outer shroud is structurally independent from the inner mercury vessel. Therefore, measurements on the outer surface, as done at J-PARC, will not give meaningful results. Based on the experience from the LANL experiment, we selected commercially available fiber optic strain sensors [3]. These sensors are small enough to fit in the interstitial space between the shroud and mercury vessel, have enough bandwidth (100kHz) to see the pressure wave, and do not suffer from electromagnetic noise from the beam and surrounding equipment. The optical sensors work on the Fabry-Perot interferometer principle, where one measures the phase shift of the light reflecting in the cavity as the length of the cavity changes along with the material, in our case the vessel wall, to which it is attached.

* ORNL is managed by UT-Battelle, LLC, under contract DE-AC05-00OR22725 for the U.S. Department of Energy. This research was supported by the DOE Office of Science, Basic Energy Science, Scientific User Facilities.
† blokland@ornl.gov

ISBN 978-3-95450-178-6

DESIGN CONSIDERATIONS

Introducing new material inside the target module requires careful consideration. The impact on its lifetime must be minimal, but it also cannot affect the existing method of detecting leaks. If there is a hole in the inner mercury vessel, the mercury will collect at the bottom of the shroud, where there are two bare wires that will now get shorted out. The newly introduced materials should not be able to short these wires nor insulate these wires. The high radiation field at the vessel wall does heat the fiber but not enough to melt it. The high radiation, between 1E12 (front) to 1E8 (back) R/hr. at 1.4 MW, also limits our choice in how to fasten the sensors. We did not find glues rated for 5000 hours at those radiation levels, and opted to use the same Stycast 2850FT epoxy that was used to glue the bare wires, thus not introducing a new material inside the interstitial space.

INSTALLATION

Optical Strain Sensors Installation

We installed eight strain sensors distributed along the vessel wall at the target's manufacturing facility [4]. The fibers were routed through a narrow, ¼ inch tube that also had to be epoxied to separate the helium gas in the interstitial space from the air around the target. The epoxy was cured using heat lamps. Figure 3 shows on the left, the curing of the epoxy; in the middle, the glued sensors on the top of the mercury vessel; on the right, the lowering of the mercury vessel into the water shroud.

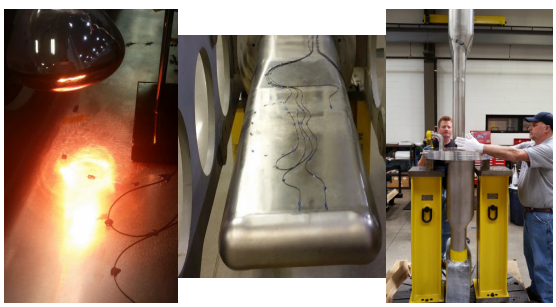

Figure 3: The installation of the optical strain sensors.

Accelerometers

Besides the optical strain sensor, we also installed two rad-hard accelerometers, one on the target mount (right behind the mercury vessel) and one on the mercury return piping several meters away from the target. These accelerometers are expected to survive much longer than the optical strain sensors.

Functional Test

To test the sensors, we drew a vacuum in the interstitial space to put a static strain on the mercury vessel to compare the sensor measurements with simulations. This test shows us not only which sensors are operational, but also how well they agree with the static strain simulation. We place high trust in the static strain calculation, as this does not involve liquid mercury dynamics.

This functional test also showed us that the new optical processor had a different scale factor than the older optical processor used in the LANL experiments. The results are shown in Figure 4. In general, the results match very well, except for sensor 6, which shows an opposite sign of strain change.

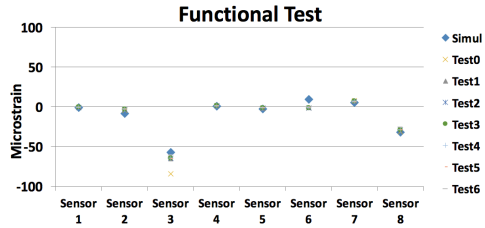

Figure 4: The functional test results.

Signal Routing from Target to Equipment

To install a new target, it must be moved into the service bay. The service bay has very high radiation levels and is contaminated. To avoid introducing contamination to the electronics, we split the cabling in two parts, one section rolls in with the target and is already connected to the sensors, while the second cable is fed from the outside to the inside of the hot cell. A connector box allows the manipulator operators to connect the two cables. Ahead of installation time, the operators practiced using a test manipulator to prepare for the actual installation. The connectors were reinforced with a metal bracket to prevent the mechanical manipulators from potentially crushing them. Even fine work, such as removing small dust caps from the fiber connectors, was performed without any problems (Fig. 5).

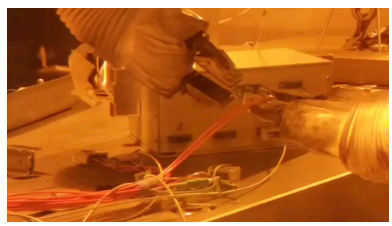

Figure 5: Manipulators connect the fiber-optic cables.

Sensors

We have now run with two instrumented targets. The first target, T13, was instrumented with eight non-rad-hard, multi-mode optical sensors, see Figure 6, and two accelerometers. The multi-mode fiber optic strain sensors are not meant for use in high radiation areas. But in our case, the residual radiation ranges from 100 to more than 100,000 Rad/hr depending on how long the beam was turned off and the location inside the target.

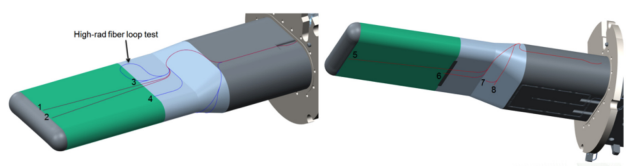

Figure 6: The layout of the installed sensors of T13.

ISBN 978-3-95450-178-6

The target is typically inserted several days before beam is turned on because all the cooling and mercury flow lines have to be connected and the accelerator has to be setup before beam can be sent to the target. Thus the sensor and fiber cables in the target are already potentially exposed up to the order of 1 MRad, even before beam has been sent to the target.

Much higher radiation resistance is to be found in single-mode fiber. To investigate super rad-hard optical fiber, we installed one run of single-mode fiber in a loop to measure transmission, and one run with a dead-end to measure the reflection as a function of radiation exposure. Laser light of milli-watt level at 1320 nm is sent through the fiber and the returned light power is measured.

For the second instrumented target, T14, we used rad-hard, high OH (hydroxyl) content, multi-mode fiber, two accelerometers, and two prototype super rad-hard, single-mode optical strain sensors developed at SNS [5].

ACQUISITION SYSTEM

To minimize signal attenuation, the cable lengths are kept as short as possible, requiring an electronics rack, equipped with accelerator timing and networking signals, to be installed in the manipulator gallery directly outside the service bay. This equipment rack holds the optical signal processor (OSP) that converts the optical signal into an analog electric signal. These electric signals, the two accelerometer signals, and the single mode fiber power signals, are all sampled by two digitizers in a PXI-crate (PCI eXtensions for Instrumentation). The software is LabVIEW based. A backup optical processor and a backup scope were installed and the data-acquisition system was thoroughly tested to make sure that we would capture the first pulse.

RESULTS

T13 Experiment

The T13 experiment started with single pulses of different intensities ranging from 10 µC to 24 µC. We also did a few pulse trains of 10 pulses to look at a possible build-up of strain. While the acquired data is immediately shown on the screens, an offline program was created to organize and analyze the data, see Figure 7.

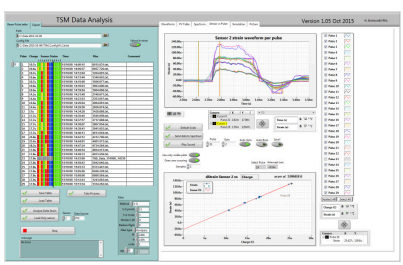

Figure 7: The offline data analysis program.

The analysis program arranges the acquired data files in columns on the left side, while on the right side it shows the strain waveforms per pulse or per sensor and can calculate the strain per beam pulse charge for each sensor by calculating the peak-to-peak strain versus intensity of several beam pulses. The program can also read simulation files and compare the measured strain waveforms to simulated strain waveforms.

T13 Multi-Mode Optical Strain Measurements

The longest lasting optical sensor, sensor 4, survived for about 80 pulses for a total of about 1.3 mC, which is equivalent to 1.5 s at 850 kW. The accelerometers survived the full production run but are also installed in a much lower radiation area. Results are shown in Figure 8 and Figure 9 and show on the top, the strain waveforms for various intensity pulses; in the middle, the fit to calculate the strain per beam pulse charge; and on the bottom, the comparision to the simulation [6]. Signals from sensors 1 and 5 should be very similar, as their locations are similar but one on top and one on the bottom. The measurements are not perfect: We see that the strain signals are failing, most likely due to radiation induced attenuation in the fiber. The output signal of the OSP starts jumping in levels and then gets a very large offset, and finally shows nothing but noise. The jumping of the signal can be seen in the sensors 3 and 5 waveforms. Sensor 6 was dead. Typically, we see a linear relation between the measured strain and beam intensity, but the intersection does not always run through zero. To further investigate, we did perform lower intensity measurements for T14.

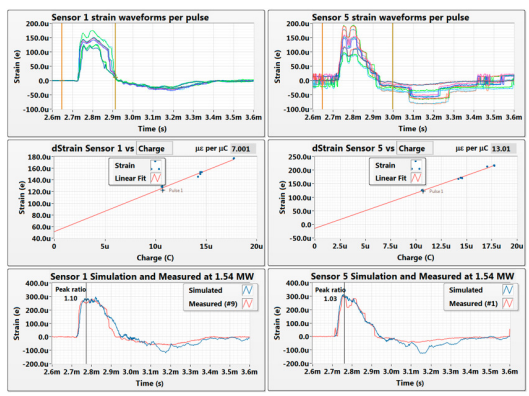

Figure 8: Results from sensors 1 and 5.

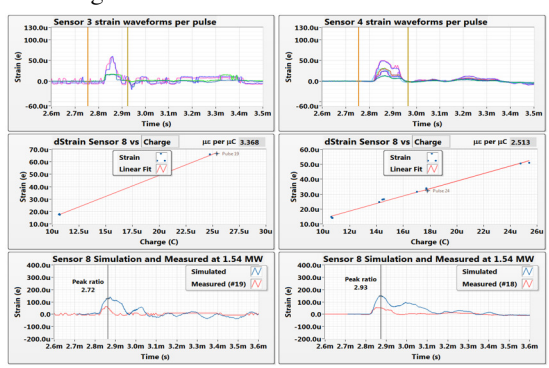

Figure 9: Results from sensors 3 and 4.

In most cases, the shape of the simulated waveform is similar to that of the measured waveform, but the two don't always agree in intensity. This can be due, e.g. in

ISBN 978-3-95450-178-6

sensor 7, to the fact that the location of the sensor is not well represented in the finite-element simulations or that it is near a simulation boundary. In some cases, the simulation results highly depend on the position, see Figure 10.

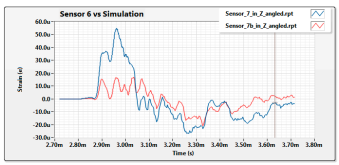

Figure 10: Simulations done near the position of sensor 7.

To look at any possible pulse-to-pulse interaction or strain build-up, we measured the strain during 10 consecutive pulses of 17.8 µC (equivalent to the 1 MW beam). Figure 11 shows the strain waveforms of sensors 4 and 8 during the 10 pulses. The signals show some reflections or resonances, but these do not seem to lead to an increase in peak-to-peak strain, and die down slowly.

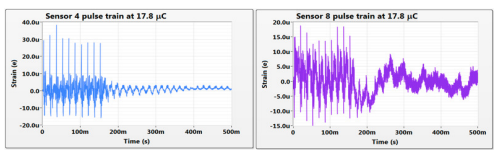

Figure 11: The pulse trains do not show a build-up.

T13 Accelerometer Measurements

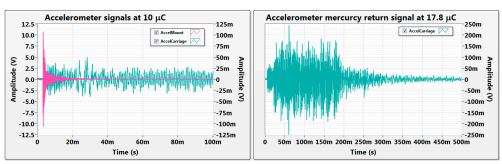

Figure 12: The signals from the accelerometers.

The accelerometer signals are shown in Figure 12. The signal of the one mounted on the mercury return is much smaller, as it is many meters away from the target and sees many reflections of the pressure wave. The accelerometer on the target mount saw good signals, but saturated at intensities above 10 µC. We have not yet derived useful information from the accelerometers from T13.

T13 Single-mode Fiber Attenuation

Figure 13 shows the attenuation as a function of time for the two fiber signals, as well as the accumulated beam energy on target. The calculated Radiation Induced Attenuation is equivalent to 0.4 dB/km/MRad and peaks at 0.9 dB/km/MRad. The peak dose amount is 83.6 GRad and the peak dose rate is 329 kRad/s at 800 kW beam power, [5]. From these results, we can estimate at least a two-week lifetime for the single-mode sensors.

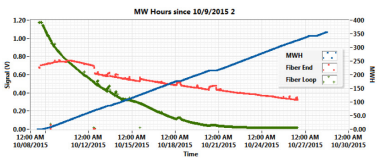

Figure 13: Attenuation of the single mode fiber.

T14 Experiment

For the T14 experiment, we replaced the regular multi-mode fiber with a high OH content multi-mode fiber that is more rad-hard. Of the 8 installed multi-mode fibers, only 5 survived the initial installation, while 2 out of 4 single-mode sensors survived. In addition, two thermocouples were installed, as shown in Figure 14. Due to the need to ensure that electrically conductive material could not reach the leak detectors, the thermocouples had to be located some distance from the beam impact area.

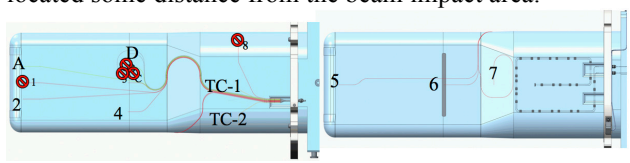

Figure 14: T14 sensor locations.

T14 Multi-Mode Optical Strain Measurements

The high OH multi-mode fiber sensor lasted beyond our expectations. The life-time of the multi-mode sensors was so much improved that the analysis program had to be rewritten to handle the large amount of data. The analysis is still in progress. We only show our initial results.

The longest performing sensors, 4 and 7, have lasted well over two weeks. Sensor 4 showed a slowly descreasing amplitude of the measured strain, but it still produced a signal for more than a month, see Figure 15. That time span is long enough to start looking for the possible breaking of the mercury vessel baffle, aka a change in the waveform. The improvement over the non rad-hard fibers is about 100,000 in terms of radiation exposure.We also found that the fibers tend to recover after a few days without beam on the target and that resetting the OSP helps regain a signal.

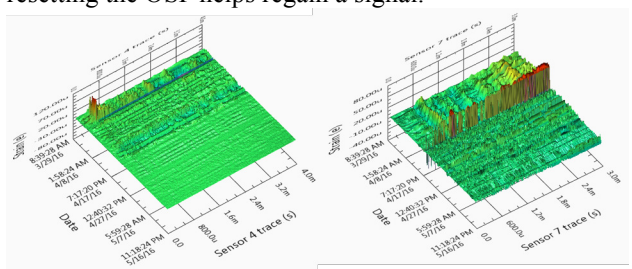

Figure 15: Lifetime of the multi-mode sensor signals.

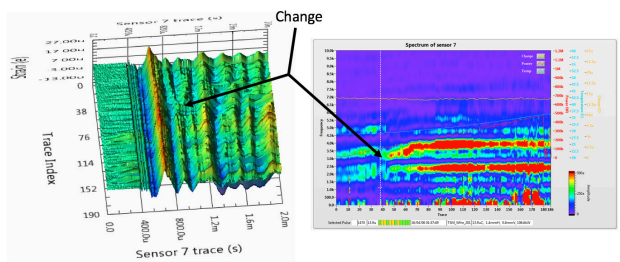

Figure 16: Possible event during ramp-up.

Figure 16 shows a change in the waveform of sensor 7 at about one week after the production start. Sensor 4

ISBN 978-3-95450-178-6

shows a similar change around the same time, April 6th at 2 am. We will investigate if this represents a change in the target's internal structure.

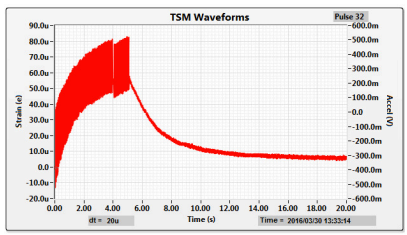

Figure 17: Build-up of static strain at 300 pulses.

An interesting result shown in Figure 17 is a static build-up of strain during a train of 300 pulses, most likely due to the local rise of the vessel temperature.

T14 Thermo-Couple Results

Figure 18 shows that the simulated and measured temperature responses are very similar, both in increase, about 0.3 C, and in decay time-constant. The temperature response is much slower than the strain response because the thermo couple is farther away from the beam impact area.

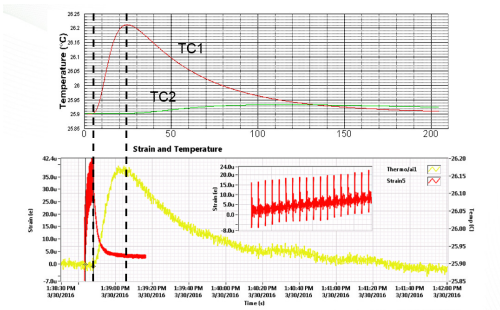

Figure 18: Simulated (top) and measured temperature (bottom) response.

T14 Accelerometer Measurements

The new accelerometer on the target mount is less sensitive than the previous ones and is no longer saturating. The data is being analyzed, but also shows some specific points in time where the signal changes.

T14 Single-Mode Optical Strain Measurements

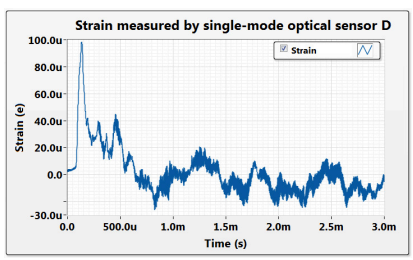

Figure 19: Single-mode fiber strain measurement.

The sensor located in the front edge of the target vessel survived for about 3 days while the sensor located in the middle of the vessel was able to provide strain measurements over 5 weeks. The signal from Sensor D is shown in Figure 19.

CONCLUSIONS

In the case of T13, we found that the strain responses are linearly proportional to the beam charge despite the non-linear (cavitating) mercury behavior, and that this is consistent with other experimental data. The simulated and measured strain data at forward and central locations, 1 and 5, agree very well in both magnitude and dynamic character, while the dynamic response is predicted well at other locations, except for sensors 7 and 8. The simulation has more high frequency content than what is observed, perhaps missing a dampening effect. The signals measured in the back are quite lower than the simulation predicted; this can be due to a dampening effect and also to the sensitivity of the simulation to location. We see some reverberation, mostly in the sensors in the back, but not build-up in the peak-to-peak response and thus at this point, we do not see an unanticipated build-up of dynamic strain endangering the life-time of the target.

We haven't fully analyzed the data from T14 yet; we are in the process of validating the single mode fiber sensor data. We do see that the temperature response is as expected.

SUMMARY

After a year-long effort by many people, we have results. While a year seems like a long time, given all the preparations and deadlines associated with target manufacturing, the time constraint in developing the measurements was actually fairly tight. The T13 instrumentation lived just long enough to give us data. We are still analyzing the T14 data. With the rad-hard, multi-mode prototype super-rad hard single-mode, we now have long-term measurement capability.

FUTURE

We plan to further develop the prototype single-mode optical strain sensors and integrate their data acquisition with the multi-mode sensors. In addition, we plan to install metal strain gauges to see if we can overcome the expected electrical noise and provide another method for measuring the strain.

ACKNOWLEDGMENTS

The authors wish to thank the many people who helped make these measurements a possibility; in particular Bob Sangrey and Jeff Bryan for the sensor installation as well as the many others who helped with tasks ranging from installing the necessary infra-structure in the manipulator gallery to cable hook-ups in the service bay.

REFERENCES

[1] B. Riemer *et al.*, "Small gas bubble experiment for mitigation of cavitation damage and pressure waves in short-pulse mercury spallation targets," *Journal of Nuclear Materials,* Volume 450 (2014) 192.

ISBN 978-3-95450-178-6

[2] T. Wan, T. Naoe, M. Futakawa, "In-situ structural integrity evaluation for high-power pulsed spallation neutron source – Effects of cavitation damage on structural vibration," *Journal of Nuclear Materials*, Volume 468, January 2016, P 321-330, ISSN 0022-3115, http://dx.doi.org/10.1016/j.jnucmat.2015.07.052.

[3] E. Pinet, "Fabry-Perot Fiber-Optic Sensors for Physical Parameters Measurement in Challenging Conditions," Journal of Sensors Volume 2009, Article ID 720980, 9 pages doi:10.1155/2009/720980.

[4] D. Winder, B. Sangrey, J. Bryan, "Target System, MTX-009 Sensor Installation," ORNL, Oak Ridge, USA,Internal Report 106010101-TR0007, Internal Report, March 2015.

[5] Liu *et al.*, "Radiation-Resistant Fiber Optic Strain Sensors for SNS Target Instrumentation", in Proc. 7th International Particle Accelerator Conference (IPAC'16), Busan, Korea, May 2016, paper MOPMR055, pp. 371-373, ISBN: 978-3-95450-147-2, doi:10.18429/JACoW-IPAC2016-MOPMR055, http://jacow.org/ipac2016/papers/mopmr055.pdf, 2016.

[6] B. Riemer, "Benchmarking dynamic strain predictions of pulsed mercury spallation target vessels," *Journal of Nuclear Materials*, Volume 343, 1 August 2005, P 81–91, doi:10.1016/j.jnucmat.2005.01.026.

ISBN 978-3-95450-178-6